Korean J. Chem. Eng., 38(12), 2560-2566 (2021)
DOI: 10.1007/s11814-021-0889-y

pISSN: 0256-1115
eISSN: 1975-7220

Preparation of polyethylene terephthalate foams at different saturation temperatures using dual methods of supercritical batch foaming

Dong Eui Kwon*, Mulugeta G. Aregay*,, Byung Kyu Park***,†, and Youn-Woo Lee*,†**

*School of Chemical and Biological Engineering & Institute of Chemical Processes, Seoul National University, 1 Gwanak-ro, Gwanak-gu, Seoul 08826, Korea
**School of Chemical and Bio Engineering, Addis Ababa Institute of Technology, King George VI St., P.O. Box 385, Addis Ababa 1000, Ethiopia
***Research Institute of Advanced Materials, Seoul National University, 1 Gwanak-ro, Gwanak-gu, Seoul 08826, Korea
(*Received 26 April 2021 • Revised 15 June 2021 • Accepted 1 July 2021*)

Abstract−Polyethylene terephthalate (PET) foams were prepared at different saturation temperatures using two supercritical foaming methods. The average cell size, cell number density, and porosity of PET foams obtained using each foaming method were compared. The crystallinity of the PET samples after the saturation step in the two-step foaming process was measured to observe the CO_2-induced crystallization. The crystallinity of PET according to the saturation temperature led to a variation in cell size in the two-step foaming. In contrast, the melting of crystals with the increase in the temperature affected the cell number density of the polymeric foam prepared by one-step foaming method. The influence of the PET crystals on the cell nucleation or cell growth in each foaming method was studied from these results.

Keywords: Polyethylene Terephthalate, Carbon Dioxide, Supercritical Foaming Process, CO_2-induced Crystallization, Heterogeneous Nucleation

INTRODUCTION

Polyethylene terephthalate (PET) foams are widely used in various applications, such as packaging materials, containers, and construction materials owing to their excellent properties including light weight, high strength and rigidity, resistance to chemicals, and good thermal, electrical and sound insulation [1,2]. In addition, recycled PET foams can be used as environmentally friendly alternatives to other polymeric foams [3,4].

Despite these excellent properties, conventional PET foaming processes present challenges because of their poor melt strength and viscosity at high temperature [5]. Since PET only flows at the temperature above melting point, several methods have been utilized to improve the melt strength, such as the use of chain extenders [6], the formation of blends with other polymer [7], and the addition of additives [3]. Apart from these methods, solid-state foaming of PET using sub- and supercritical CO_2 has also been studied to avoid the melting state in the process.

Since crystals in semi-crystalline polymers such as PET act as heterogeneous nucleation sites in the foaming process, the cell number density of polymer foams increases with an increase in the number of crystals [8]. Furthermore, the crystals in PET are associated with an increase in the melt strength, which can be helpful in building and maintaining pore structure [9,10]. Those effects of crystals in PET have significance especially in one-step foaming process and supercritical extrusion, in which the cell formation is induced by depressurization at high temperature. However, the two-step foaming process, in which the pore structure is obtained by expanding the supersaturated blowing agent after depressurization, does not benefit from the crystals because of their low CO_2 affinity and stiffness. When amorphous PET is exposed to a high-pressure CO_2 environment, the swelling and plasticization effect of the CO_2 dissolved in the polymer matrix facilitates chain mobility. Therefore, the crystallization of semi-crystalline polymers occurs even at low temperature, which is defined as CO_2-induced crystallization [11]. The crystals formed during the saturation process lower the amount of CO_2 dissolved in the polymer and consequently hinder the cell growth in the two-step foaming process.

For these reasons, several studies have been conducted to produce PET foams through a two-step foaming process using CO_2 to overcome the disadvantages of crystallization. PET foams were prepared by inducing cell growth at relatively high foaming pressure or temperature compared to amorphous polymers to overcome the rigidity of the crystalline region [12]. Furthermore, Yuan et al. studied CO_2-induced crystallization at ambient temperature and observed the pore structure in the amorphous and crystalline layers formed during the sorption process [13]. The periodical CO_2 sorption process was applied to PET foaming to control the crystallinity by Zhao et al. [14]. The sorption and depressurization processes were repeated several times to limit the crystallization, resulting in an increase in the diffusion and dissolution of CO_2 in the polymer. From these previous studies, it is essential for the fabrication of PET foams using CO_2 to investigate the crystal structure of PET in CO_2 environment. However, PET foams have not been prepared

†To whom correspondence should be addressed.
E-mail: bkpark@snu.ac.kr, ywlee@snu.ac.kr

with different saturation temperatures in both two-step foaming and one-step foaming methods to investigate the influence of the variation crystal structures on foam structures with different CO_2 temperature.

Therefore, we prepared the PET foam using CO_2 at different temperatures in both foaming methods. The effect of saturation temperature on the PET foam induced by two-step foaming or one-step foaming was investigated based on the average cell size, cell number density, and porosity. Each pore formed in the amorphous or crystalline region in the PET matrix was observed in two-step foaming according to the degree of CO_2-induced crystallization at different saturation temperatures. Also, PET foams were produced by one-step foaming near melting point of PET to study the effect of crystal melting behavior on cell structure.

EXPERIMENTAL

1. Materials

The PET amorphous sheet (ES303010) was purchased from Goodfellow. The sheet was cut into 2×2 cm squares, with a thickness of 1 mm. Carbon dioxide (purity: >99.95%) used as a blowing agent was purchased from Hyupshin Gas Industry.

2. Saturation and Foaming Methods

Polymeric foams were prepared using two different processes. The first is a two-step foaming process, in which the expansion of CO_2 highly dissolved in polymer is induced by increasing the temperature. The other is a one-step foaming process, which creates the foams by rapidly releasing the pressure from the polymer exposed to CO_2 at a high temperature and pressure.

Two-step foaming was conducted through a saturation process of injecting CO_2 into the polymer and a foaming process of expanding the injected CO_2 to form a pore. The saturation process was as follows. PET sheets were placed in a vessel. Then the vessel was placed in a bath at the desired temperature. CO_2 was delivered into the vessel using a plunger pump (HKS-12000, HY Accuracy). The inner pressure of the vessel was maintained at 10 MPa, and the saturation temperature was 0, 25, and 50 °C. Subsequently, the vessel was placed for seven days at a saturation temperature of 0 °C, two days at 25 °C, and 16 h at 50 °C. The foaming process was performed after the saturation steps. The vessel was depressurized within 1 s, and the specimens from the vessel were immersed in a medium at 100, 150, 200 and 225 °C for 3 min. Ethylene glycol was used as the medium at 100 and 150 °C, and emulsifiable oil at 200 and 225 °C. Finally, the samples were quenched in a water/ethanol mixture at a temperature below 0 °C for no further progress.

One-step foaming was conducted as follows. CO_2 was introduced into a 23 ml vessel containing the PET sheet. The injected CO_2 was then weighed on a scale (EPG214, OHAUS). The weight of CO_2 was calculated based on the density of CO_2 at 30 MPa, and the temperatures of 225, 230, 235, and 240 °C. The density of CO_2 was obtained from the NIST WebBook [15]. Subsequently, the vessel was immersed in a salt bath at the desired temperature of 225, 230, 235 and 240 °C for 30 min, and the pressure was released within 1 s. After depressurization, the vessel was quenched in cold water. The prepared PET was removed from the vessel and dried at room temperature.

3. Measurement of Crystal Structures

Differential scanning calorimetry (DSC, Q100, TA Instrument) was used to measure the crystallinity of PET by CO_2-induced crystallization. After the saturation process, the PET sheets were kept at −20 °C to inhibit the cell growth. Then, each sample was pulverized into powder using freezer milling (Freezer/Mill 6770, SPEX SamplePrep). Approximately 3 mg of powder was heated to 300 °C at a rate of 5 °C/min under N_2 environment. The cold crystallization enthalpy (ΔH_{cc}) was measured from the exothermic peak at near 130 °C, and the melting enthalpy (ΔH_m) from endothermic peak at near 250 °C. The melting enthalpy of 100% crystalline PET ($\Delta H_{m,0}$) was 140 J/g [16]. The crystallinity of PET (X_c) was calculated from the enthalpy using Eq. (1).

$$X_c = 100 \times \frac{\Delta H_m - \Delta H_{cc}}{\Delta H_{m,0}} \tag{1}$$

X-ray diffraction analysis (XRD) was performed to observe the crystal structure, such as crystallite size in high temperature near melting point. PET powder was analyzed using power X-ray diffractometry (D8 Advance, Bruker) equipped with Cu-Kα radiation (1.5418 Å). Diffraction data were obtained in 2θ range from 5 to 50° with the step size 0.0204°/step and scan rate 2 step/s.

4. Foam Characterization

The prepared foam was observed by using a field-emission scanning electron microscope (FE-SEM, SIGMA, Carl Zeiss, Germany). Polymeric foam specimens were fractured after freezing in liquid N_2 for 5 min to observe the cross section of the obtained foams. Thereafter, the surface was coated with platinum using a sputtering coater (SCD005, BAL-TEC) and analyzed using FE-SEM. The SEM images were analyzed by Image J and the Morpholib J library to calculate the cell size and the cell number density. Assuming that the pore is circular, each diameter was calculated from the area of the cell observed in the images. More than 300 cells were counted for each polymeric foam to obtain an average. To calculate the cell number density (N_{cell}), the number of cells (N) in a specific area (A) in the SEM images was counted. N_{cell} is defined as the number of cells per volume of the polymer matrix except the void fraction, and was calculated by Eq. (2)

$$N_{cell} = \left(\frac{N}{A}\right)^{\frac{3}{2}} \left(\frac{\rho_0}{\rho_f}\right) \tag{2}$$

where, ρ_0 is the density of raw PET, and ρ_f is the density of the PET foam.

The density (ρ) of the foamed polymer was measured from ASTM D792-00, and calculated using Eq. (3),

$$\rho = \frac{a}{a + w - b} \rho_{water} \tag{3}$$

where, a is the weight of the sample in air, b is the weight of the sample immersed in water with a sinker, and w is the weight of the sinker in water. ρ_{water} was assumed to be 1 g/ml. The porosity (ϕ), which is the void fraction of polymeric foam, was obtained from the density of raw and foamed PET using Eq. (4).

$$\phi = 1 - \frac{\rho_0}{\rho_f} \tag{4}$$

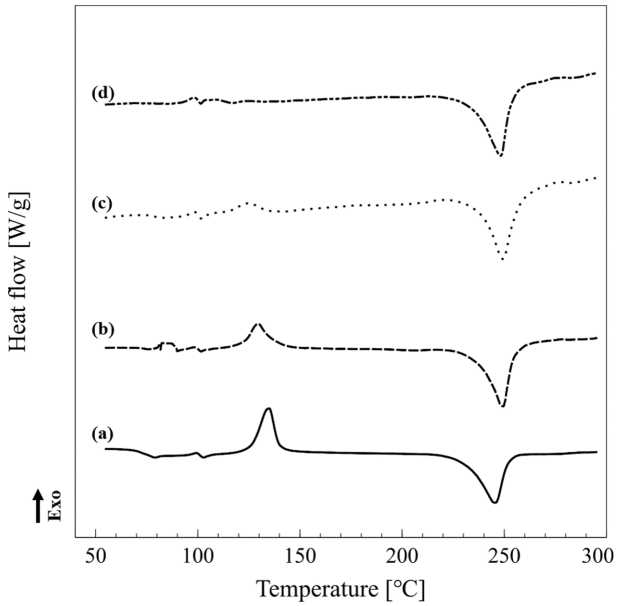

Fig. 1. DSC thermograms of (a) raw PET and samples after being exposed to CO_2 at 10 MPa, (b) 0 °C, (c) 25 °C, and (d) 50 °C.

RESULTS AND DISCUSSION

1. CO_2-induced Crystallization of PET in the Saturation Process

Fig. 1 shows the thermograms of PET samples at different saturation temperatures. The cold crystallization peak near 130 °C disappeared as the saturation temperature increased. This indicates that the amorphous region in the polymer matrix diminished when treated at a high saturation temperature. CO_2-induced crystallization is caused by the swelling and plasticization of semi-crystalline polymers due to the high absorption of CO_2 [11,17]. However, the crystallinity of PET in the 0 °C CO_2 environment did not increase as much as that in the high saturation temperature (Table 1), because excessive free volume and chain mobility by strong plasticization at low temperature inhibited the formation of the crystalline region [18]. Hence, PET saturated with 0 °C of CO_2 was relatively amorphous compared to PET samples saturated at higher temperature.

Table 1. Crystallinities of PET samples after CO_2 saturation

Sample	Saturation temperature [°C]	ΔH_{cc} [J/g]	ΔH_m [J/g]	X_{cc} [%]
Raw	-	19.07	31.70	9.01
1	0	14.14	38.40	17.34
2	25	4.64	42.05	26.72
3	50	0.00	42.12	30.09

2. Effect of Temperature on Foam Morphology in Two-step Foaming

Fig. 2 shows SEM images of PET foams prepared by the two-step foaming at various saturation temperatures. The cell size varied from 10 to 50 μm with the temperature. Foams at saturation

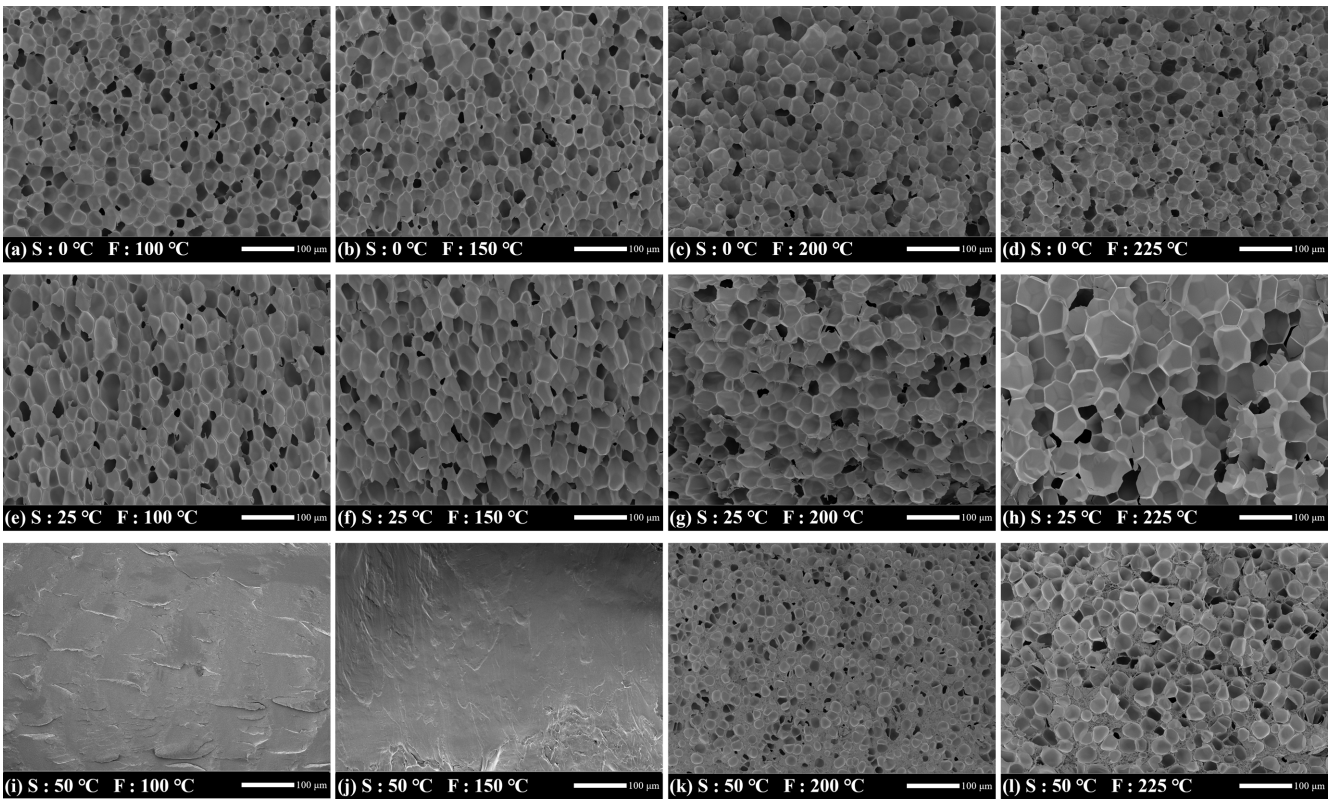

Fig. 2. SEM images of PET foams prepared by two-step foaming. Each sample was saturated with CO_2 at 10 MPa, 0 °C (a)-(d), 25 °C (e)-(h), and 50 °C (i)-(l), and then foamed at 100, 150, 200, and 225 °C.

Table 2. Experimental conditions of PET foams

Sample[a]	Saturation pressure [MPa]	Saturation temperature [°C]	Foaming temperature [°C]	Cell size[b] [μm]	Cell number density [10^8 Cells/cm^3]	Porosity [%]
2	10	0	100	23.76 (7.12)	5.67 (0.99)	80.71 (1.10)
2	10	0	150	28.41 (7.50)	5.58 (1.36)	87.44 (0.61)
2	10	0	200	29.29 (7.67)	7.97 (1.99)	91.54 (0.35)
2	10	0	225	25.92 (5.61)	9.62 (1.59)	88.79 (1.38)
2	10	25	100	29.60 (6.35)	2.03 (0.15)	69.17 (5.96)
2	10	25	150	33.33 (7.08)	2.99 (0.02)	82.11 (4.50)
2	10	25	200	35.91 (8.63)	3.56 (0.48)	88.49 (1.59)
2	10	25	225	51.95 (12.75)	1.20 (0.08)	89.56 (0.34)
2	10	50	100	-	-	-
2	10	50	150	-	-	-
2	10	50	200	15.21 (3.40)	4.66 (0.93)	58.63 (3.42)
2	10	50	225	24.01 (5.35)	6.17 (1.45)	81.64 (0.12)
1	30	225	225	10.36 (2.08)	6.58 (1.49)	29.76 (2.89)
1	30	230	230	12.90 (2.26)	11.02 (0.19)	54.86 (0.56)
1	30	235	235	12.71 (2.13)	32.38 (4.01)	76.06 (2.32)
1	30	240	240	21.32 (5.38)	1.96 (0.28)	53.60 (5.28)

[a]2 indicates the foams formed by two-step foaming, and 1 indicates the foams formed by one-step foaming.
[b]Standard deviations of cell size, cell number, and porosity were presented in parentheses

temperatures of 0 and 25 °C were fabricated at relatively low foaming temperature, whereas PET saturated with CO_2 at 50 °C was not foamed below 150 °C as shown in Fig. 2(i) and (j). Table 1 shows that the crystallinity of PET after the saturation process was high at 50 °C. This indicates that the high crystallinity of PET hindered cell expansion. The experimental conditions with the corresponding average cell size, cell number density, and porosity are listed in Table 2.

Fig. 3 shows the average cell size of the PET foams under different saturation conditions. At a saturation temperature of 0 °C, the cell size converged to a range of 25 to 30 μm as the foaming temperature varied. The average cell size foamed at 100 °C was 23.76 μm, and it had similar values with average size (22.31 μm) and crystallinity (14.34%) of PET foams prepared by Zhao et al., which was saturated with CO_2 at 10 °C, 6 MPa and foamed at the same foaming temperature [14]. While the average cell size of foams at 25 °C and 50 °C increased as foaming temperature increased. The cell size at 25 °C slightly increased from 30 to 35 μm, and then sharply increased when the foaming temperature reached 225 °C. A similar correlation was observed at the saturation temperature of 50 °C. Table 1 shows the crystallinity of PET at different saturation temperature. The difference in crystallinity caused the variation in the average cell size of each foam. PET specimens saturated with CO_2 at 0 °C were not affected by the crystalline region due to low crystallinity; therefore the average cell size was not varied much. On the other hand, more crystalline PET after saturation at 50 °C either had relatively small pores or were not foamed because of the stiffness of the crystals. However, the average cell size sharply increased at 225 °C, because the low viscosity of the polymer and the high expansion of CO_2 at high temperature overcame the resistance of crystals. The average cell size of the PET foam obtained at 25 °C saturation was larger than that obtained at other saturation temperature. Since the crystal provided a heterogeneous nucleation site [19], the growth occurred intensely from the formed nuclei. Despite similar crystallinity with 50 °C, swelling due to higher CO_2 uptake at 25 °C weakened the crystalline structure that suppressed the cell growth. Thus, nuclei from heterogeneous nucleation had sufficient cell growth to form a larger cell through coalescence [20], unlike foams at 50 °C which had independent cell growth because of the restriction by crystals. The decrease of viscosity induced by plasticization effect facilitated the cell growth in two-step foaming.

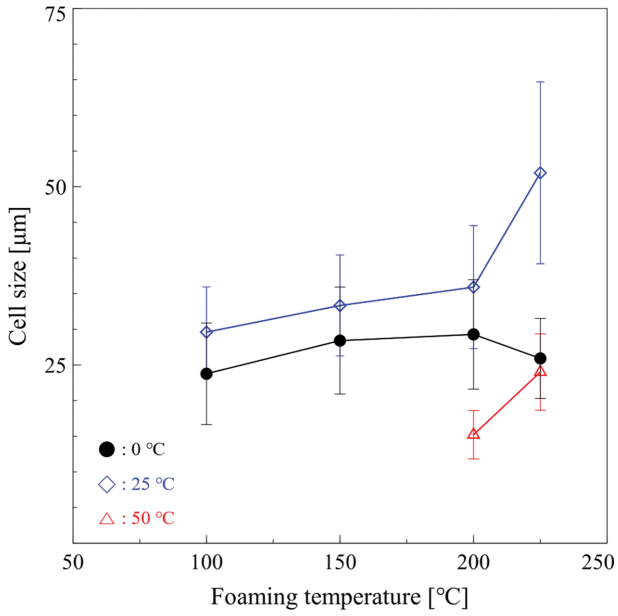

Fig. 3. Average cell size of PET foams prepared by two-step foaming at the different saturation temperatures.

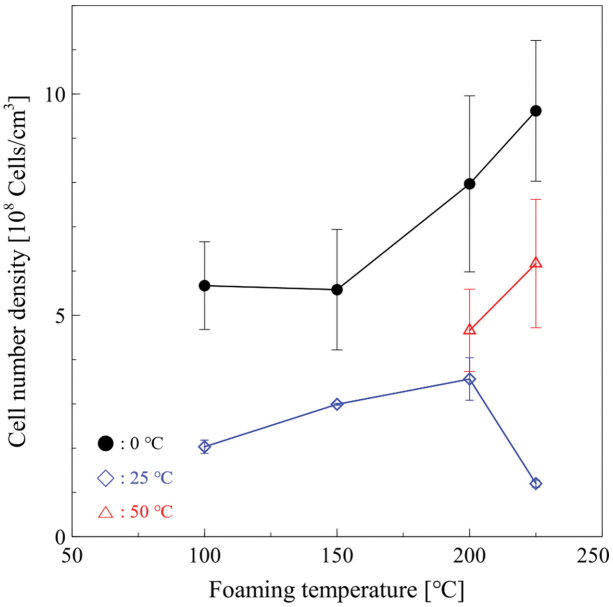

Fig. 4. Cell number density of PET foams prepared by two-step foaming at the different saturation temperatures.

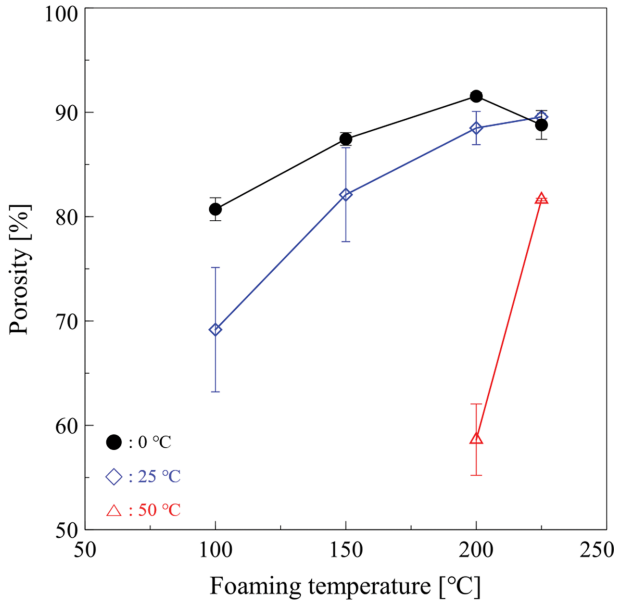

Fig. 5. Porosity of PET foams prepared by two-step foaming at the different saturation temperatures.

Plasticization is more likely to occur at high temperature or high CO_2 uptake in polymer [21]. However, since CO_2 concentration decreased with the increase of saturation temperature at given CO_2 pressure, plasticization had the opposite effect when increasing saturation temperature, the increase by higher temperature and the decrease by lowering CO_2 concentration. Therefore, the cell growth was restricted by weak plasticization because of the low temperature at 0 °C and the low CO_2 concentration and high crystallinity at 50 °C. Otherwise, larger cells could be formed in the saturation temperature of 25 °C due to the strong plasticization by relatively high temperature and CO_2 concentration.

Fig. 4 shows the cell number density of each PET foam. The cell number density was highest at 0 °C and lowest at 25 °C. The amount of saturated CO_2 increased as the CO_2 temperature decreased, despite the slow process time [22,23]. As more cell nucleation is induced by a higher CO_2 concentration [24], the PET samples at 0 °C, which had the highest CO_2 uptake, had the largest number of cell density. On the other hand, the cell number density at 25 °C was lower than that at 50 °C, which had a lower CO_2 concentration. This was because CO_2 was consumed more to raise the pore size than to form a cell nucleus.

Fig. 5 shows the porosity of PET foams. The porosity increased with a decrease in saturation temperature. This is a result of the CO_2 concentration in the polymer matrix. Since porosity is defined as the void fraction of polymeric foams, it has a high value at either a large average cell size or a high cell number density. Supersaturated CO_2 after depressurization was consumed by both the formation of cell nuclei and the cell expansion; thus, the amount of CO_2 in the polymer largely influenced the porosity of the polymeric foams [25]. Meanwhile, under the same saturation condition, the porosity increased as foaming temperature increased. This means that more CO_2 participated in the process at higher temperature. At a low foaming temperature, the cell nuclei after depressurization disappeared without growing enough to maintain the structure because the expansion could not displace the enveloping crystalline region. However, strengthening the expansion of CO_2 and weakening the viscosity of the polymer matrix at high temperature facilitated the formation and growth of foams [26,27]. Consequently, the porosity increased with an increase in cell size or cell number density at high foaming temperature.

3. Effect of Temperature on Foams in One-step Foaming

Fig. 6 shows SEM images of PET foams prepared by one-step foaming at various temperatures. PET samples by one-step foaming did not form a cell structure below 225 °C, and did not main-

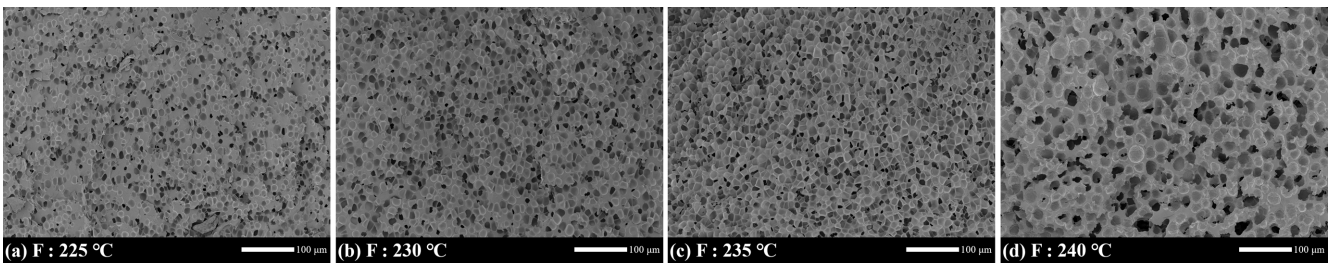

Fig. 6. SEM images of PET foams manufactured by one-step foaming.

tain the structures over 240 °C due to the temperature. PET foams prepared by one-step foaming between 225 and 240 °C had the cells in the range of 10-20 μm, which are relatively small pores compared with those prepared by the two-step foaming method. As the temperature increased, the wall between pores became thinner. However, the cell structure at 240 °C was quite ruptured in spite of relatively large pores because the structure could not withstand the high temperature near the melting point.

Fig. 7 shows the average cell size of PET foams at the different foaming temperatures. The cell size did not show significant variation in the temperature range from 225 to 235 °C, but it sharply increased to 20 μm at 240 °C. This was because of cell coalescence as enveloping walls collapsed at the high temperature near melting point [20]. Unlike the similar cell sizes at different temperatures except 240 °C, the cell number densities rose steeply (Fig. 8). The increase would came from the heterogenous nucleation [28,29]. As shown in Fig. 1, the PET sample melted gradually at a range from 220 °C to 250 °C; therefore, a number of crystals were formed by splitting the crystal structures with increasing temperature. Since these molten crystals acted as a heterogeneous nucleation site [30,31], the cell nucleation was more induced. In XRD pattern of Fig. 10,

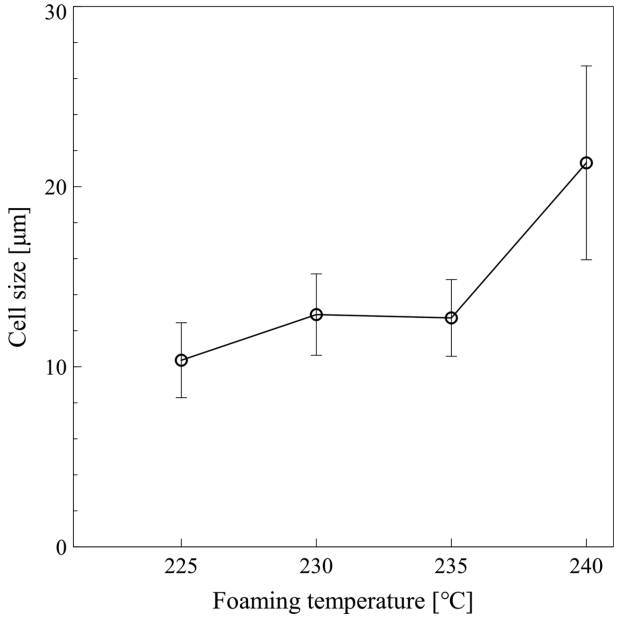

Fig. 7. Average cell size of PET foams prepared by one-step foaming at the temperature of 225 °C, 230 °C, 235 °C, and 240 °C.

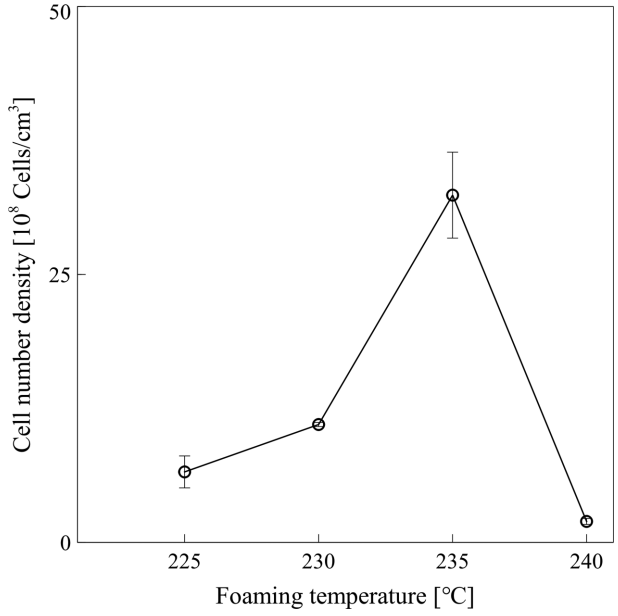

Fig. 8. Cell number density of PET foams prepared by one-step foaming at the temperature of 225 °C, 230 °C, 235 °C, and 240 °C.

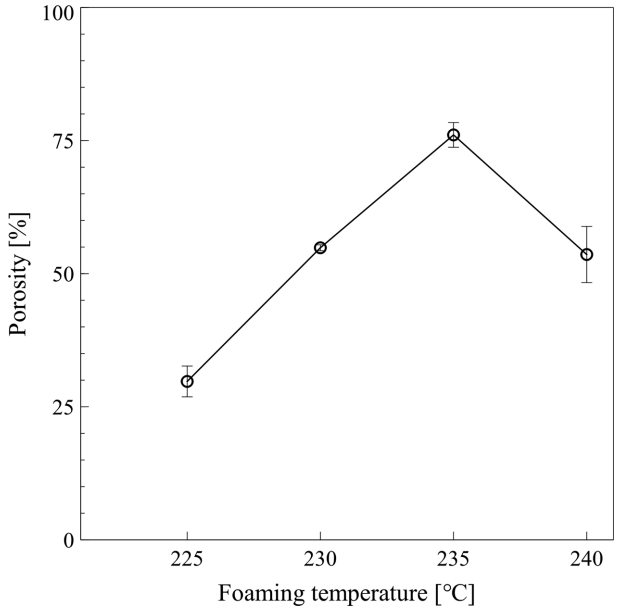

Fig. 9. Porosity of PET foams prepared by one-step foaming at the temperature of 225 °C, 230 °C, 235 °C, and 240 °C.

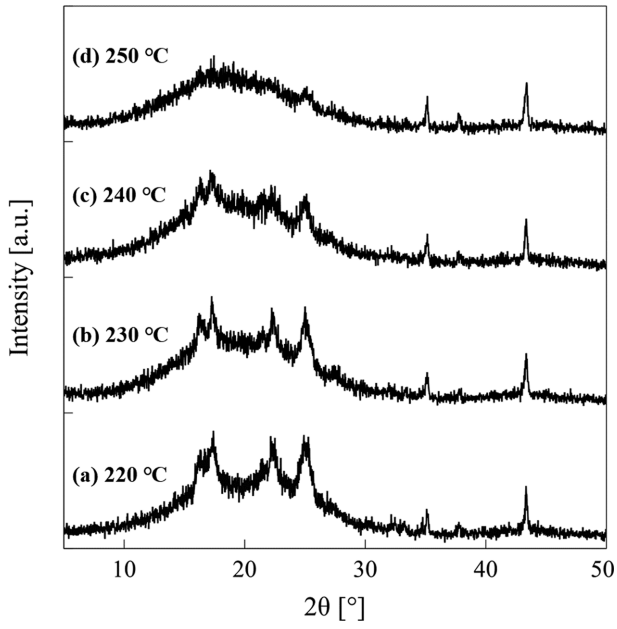

Fig. 10. XRD patterns of PET near melting point.

the intensity of crystal peak (16.3°, 17.3°, 22.4°, 25.0°) was weaker and broader as close to the melting point. From the Scherrer equation, the crystallite size is smaller at the broader peak; therefore, numerous small crystals were formed as the temperature increased [32]. Since numerous small crystals provided more heterogeneous nucleation sites, it made the cell number increase at higher foaming temperature in one-step foaming. When the temperature reached 240 °C, where the crystal structure nearly melted, the boundaries of the cells did not have enough strength to support the shape of the cells [33]. Hence, the cell number density at 240 °C decreased due to cell collapse.

The porosity of PET foams by one-step foaming was proportional to the cell number density as shown in Figs. 8 and 9. As the average cell sizes of the foams at 225 to 235 °C were similar, the porosity changed as the cell number density varied. Although the foam at 240 °C had a relatively large cell size compared with those at other temperatures, the porosity was lower than that at 235 °C owing to the low cell number density.

CONCLUSION

PET foams using two different foaming methods were prepared at various saturation temperatures. CO_2-induced crystallization occurred during the saturation step in the two-step foaming method because of the large amount of CO_2 dissolved in the polymer matrix at low temperature. Cell growth should overcome the restriction of the crystals by the expansion of the dissolved CO_2 in the two-step foaming method. Hence, the variation of the average cell size of PET foams was shown according to the crystallinity at the different saturation temperatures. On the other hand, the saturation temperature has a significant effect on the cell number density in one-step foaming. Since the semi-molten crystals near melting point provide a number of heterogeneous nucleation sites, the cell number density varied with increasing the temperature in the one-step foaming method. Hence, it was concluded that the cell growth largely depended on the saturation temperature in two-step foaming, whereas cell nucleation was affected by the temperature in one-step foaming. Considering that the existence of crystals in semi-crystalline polymers is important in the supercritical foaming process, this work will be helpful for the preparation of semi-crystalline polymer foams using both foaming methods using CO_2 as a blowing agent.

ACKNOWLEDGEMENTS

This research was supported by the Institute of Engineering Research at Seoul National University and Grant (NRF-2018R1A2B2008196) from National Research Foundation of Korea funded by Ministry of Science and ICT of Korea government.

REFERENCES

1. L. Sorrentino, E. Di Maio and S. Iannace, *J. Appl. Polym. Sci.*, **116**, 27 (2010).
2. R. Guan, B. Wang, D. Lu, Q. Fang and B. Xiang, *J. Appl. Polym. Sci.*, **93**, 1698 (2004).
3. C. C. Lai, C. T. Yu, F. M. Wang, H. T. Hsiao, W. C. Liang, Y. H. Ho, W. F. Teng, L. C. Liu and C. M. Chen, *Polym. Test.*, **74**, 1 (2019).
4. M. Bedell, M. Brown, A. Kiziltas, D. Mielewski, S. Mukerjee and R. Tabor, *Waste Manag.*, **71**, 97 (2018).
5. M. Xanthos, U. Yilmazer, S. K. Dey and J. Quintans, *Polym. Eng. Sci.*, **40**, 554 (2000).
6. H. Guo, K. Nadella and V. Kumar, *J. Mater. Res.*, **28**, 2374 (2013).
7. D. E. Kwon, B. K. Park and Y. W. Lee, *Polymers* (Basel), **11**, 291 (2019).
8. J. Ni, K. Yu, H. Zhou, J. Mi, S. Chen and X. Wang, *J. Supercrit. Fluids*, **158**, 104719 (2020).
9. S. Yao, D. Hu, Z. Xi, T. Liu, Z. Xu and L. Zhao, *Polym. Test.*, **90**, 106649 (2020).
10. V. Kumar, R. P. Juntunen and C. Barlow, *Cell. Polym.*, **19**, 25 (2000).
11. J. S. Chiou, J. W. Barlow and D. R. Paul, *J. Appl. Polym. Sci.*, **30**, 3911 (1985).
12. M. T. Liang and C. M. Wang, *Ind. Eng. Chem. Res.*, **39**, 4622 (2000).
13. D. Li, T. Liu, L. Zhao and W. Yuan, *AIChE J.*, **58**, 2512 (2012).
14. T. Xia, Z. Xi, T. Liu and L. Zhao, *Chem. Eng. Sci.*, **168**, 124 (2017).
15. E. W. Lemmon, M. O. McLinden and D. G. Friend, Thermophysical Properties of Fluid Systems in NIST Chemistry WebBook, NIST Standard Reference Database Number 69, P. J. Linstrom and W. G. Mallard, National Institute of Standards and Technology, Gaithersburg (2021).
16. A. Mehta, U. Gaur and B. Wunderlich, *J. Polym. Sci. Polym. Phys. Ed.*, **16**, 289 (1978).
17. A. Jomekian, B. Bazooyar, S. J. Poormohammadian and P. Darvishi, *Korean J. Chem. Eng.*, **36**, 2047 (2019).
18. Y. Yang, X. Li, Q. Zhang, C. Xia, C. Chen, X. Chen and P. Yu, *J. Supercrit. Fluids*, **145**, 122 (2019).
19. D. F. Baldwin, C. B. Park and N. P. Suh, *Polym. Eng. Sci.*, **36**, 1437 (1996).
20. A. Kumar, B. Patham, S. Mohanty and S. K. Nayak, *J. Polym. Res.*, **26**, 80 (2019).
21. E. Di Maio and E. Kiran, *J. Supercrit. Fluids*, **134**, 157 (2018).
22. H. Guo and V. Kumar, *Polymer* (Guildf), **57**, 157 (2015).
23. T. J. Yoon, W. Kong, D. E. Kwon, B. K. Park, W. I. Lee and Y. W. Lee, *J. Supercrit. Fluids*, **124**, 30 (2017).
24. R. Li, J. H. Lee, C. Wang, L. Howe Mark and C. B. Park, *J. Supercrit. Fluids*, **154**, 104623 (2019).
25. Y. K. Kwon and H. K. Bae, *Korean J. Chem. Eng.*, **24**, 127 (2007).
26. V. Kumar and J. E. Weller, *Int. Polym. Process.*, **8**, 73 (2013).
27. I. K. Hong and S. Lee, *Korean J. Chem. Eng.*, **31**, 166 (2014).
28. J. Hou, G. Zhao, G. Wang, L. Zhang, G. Dong and B. Li, *J. Supercrit. Fluids*, **145**, 140 (2019).
29. Y. W. Chang, S. Kim, S. C. Kang and S. Y. Bae, *Korean J. Chem. Eng.*, **28**, 1779 (2011).
30. C. Jiang, S. Han, S. Chen, H. Zhou and X. Wang, *Cell. Polym.*, **39**, 223 (2020).
31. M. Nofar, E. Büşra Küçük and B. Batı, *J. Supercrit. Fluids*, **153**, (2019).
32. A. M. Hindeleh and D. J. Johnson, *Polymer* (Guildf), **19**, 27 (1978).
33. Y. Srithep and L. S. Turng, *J. Polym. Eng.*, **34**, 5 (2014).